

RESEARCH

Open Access



Effects of Temperature and Stress on Creep Behavior of PP and Hybrid Fiber Reinforced Reactive Powder Concrete

Xiaomeng Hou^{1,2*} , Muhammad Abid^{1,2,3}, Wenzhong Zheng^{1,2} and Raja Rizwan Hussain⁴

Abstract

Reactive powder concrete (RPC) is an advanced cementitious material with ultra-high strength, remarkable durability and excellent toughness. However, temperature dependent creep is a major concern as very little work has been reported in the literature. Therefore, systematic investigations are still missing in state of the art. This paper focuses on the impact of Polypropylene (PP) and hybrid (steel and PP) fibers on creep behavior of RPC at elevated temperature. Temperature-dependent creep is further characterized into free thermal strain (FTS), short-term creep (STC) and transient strain (TS), based on different thermo-mechanical regimes. Varying heating and loading schemes were considered such as steady-state and transient thermo-mechanical conditions. The target temperatures considered for steady-state thermal conditions and transient case are 120, 300, 500, 700 and 900 °C. Compressive strength was considered up to 60% load ratio of ambient and temperature dependency. The result shows that STC increases with increasing stress level and higher target temperature. The increase in STC becomes obvious above the transition stage of quartz aggregate. Furthermore, HRPC have significantly higher STC than PRPC and other traditional types of concretes. The evolution of FTS and TS was quite slow below 250 °C. However, at high temperature significant increase in FTS and TS were observed. Furthermore, increasing stress level and the addition of steel fibers results in high TS. Overall, the performance of PP fiber was better than the hybrid fibers on the creep behaviour of RPC. Finally, constitutive relationships were proposed for FTS, STC and TS, which will be used as input data in numerical models of fire resistance calculations.

Keywords: reactive powder concrete (RPC), PP fiber, hybrid fiber, short-term creep (STC), transient strain (TS), fire safety design

1 Introduction

Reactive powder concrete (RPC) is an advanced generation of concrete. RPC is among highly used types of ultra-high performance concretes. It was originally developed in early 1990s by Bouygues's laboratory (Richard and Cheyrezy 1994). The performance of RPC is superior to traditional types of concretes in term of ultra-high strength, excellent durability and high fracture energy (Hou et al. 2018; Yu et al. 2018). The improved

performance of RPC is because of micro-structural development techniques, which includes elimination of coarse particles, incorporation of very small particles of silica fume to fill the interstitial gaps between quartz sand and unhydrated cement particles, addition of fibers, replacing traditional sand with reactive quartz sand and special curing methods at high temperature and pressure (Richard and Cheyrezy 1995; Cheyrezy et al. 1995). The latest generation of superplasticizer is used for effective compensation of low fluidity and better dispersion of particles (Sanchayan and Foster 2016). Over the last two decades, RPC has been commercially used in the construction of tunnels, bridges, runways, parking aprons of airports, nuclear structures and industrial structures, around the world (Bierwagen and Abu-Hawash 2005;

*Correspondence: houxiaomeng@gmail.com

¹ Key Lab of Structures Dynamic Behavior and Control of the Ministry of Education, Harbin Institute of Technology, Harbin 150090, China
Full list of author information is available at the end of the article
Journal information: ISSN 1976-0485 / eISSN 2234-1315

Graybeal 2004). Some of these structures are exposed to thermal fatigue such as parking apron of airports and industrial structures (Bamonte and Gambarova 2009). Nuclear structures are also exposed to high temperature. Furthermore, accidental structural fire may cause severe damage to structures. Therefore, this study will cover-up the knowledge gap about the creep behavior of fiber reinforced RPC at high temperature.

In spite of outstanding performance at ambient temperature, RPC may be subjected to fire-induced spalling at high temperature due to its compact microstructure. Fibers plays important role in protecting RPC from spalling under high temperature. The incorporation of proper dosage of polypropylene (PP) and steel fiber combat this problem (Zheng et al. 2012, 2014; Hou et al. 2019a, b).

However, different types of fibers have totally different effect on the strength and fire resistance behavior of RPC. Steel fibers are more effective to improve not only compressive but tensile strength of RPC. Thus the internal built-up pressure can be resisted effectively and RPC fire-resistance behavior can be improved. PP fibers result in decrease in the strength of RPC due to their low elastic modulus. However, they melt at 167 °C and left micro-channels which releases the internal pressure and thus RPC withstands high temperature without bursting. The more effective way is the hybrid combination of steel and PP fibers which has not only being proved to be effective at materials level (Abid et al. 2017, 2019a) but also their full scale beams did not spalled under high temperature (Hou et al. 2019a, b). Creep behavior of RPC at high temperature is an open question, since very little information is available about it. Creep of Steel fiber reinforced RPC at high temperature was investigated by Abid et al. (2019b). Results showed that creep increased with increasing stress level and temperature. Since different fibers types have different effects/mechanism under high temperature, therefore their high-temperature creep behavior should be studied separately for RPC.

The creep behavior at high temperature is characterized based on different thermo-mechanical regimes. The expansion or contraction of concrete without load is called free thermal strain (FTS) (Rilem 1997). Whereas, the strain at steady-state thermo-mechanical condition is called basic creep, steady-state creep or short-term creep (hereafter referred as STC) (Rilem 2000). Furthermore, strain in the excess of thermo-elastic behavior under constant load during virgin heating is called transient creep strain or transient strain (TS) (Rilem 1998; Torelli et al. 2016).

In the last few decades, extensive studies were carried out about the creep behavior of normal strength concrete (NSC), and high strength concrete (HSC)

high-performance concrete (HPC). Among the pioneers, Anderberg and Thelandersson (1976) investigated creep behavior of NSC at high temperature. Their concrete was made from siliceous aggregate with water to cement ratio (w/c) of 0.6. It was observed that FTS and TS were not affected by changing heating rate. The relationship of FTS with temperature was linear. Similarly, TS was also found out to be linear when constant load was maintained during heating. However, a FTS dependent linear model was proposed for TS.

Khoury et al. (1985a) divided the total creep into free thermal strain (FTS) and load-induced thermal strain (LITS). LITS was further separated into basic creep, elastic creep and transient creep. The transient creep consists of transitional thermal creep (TTC) and drying creep, however, TTC is the main component of transient creep. It was observed that the expansion of concrete was mainly affected by aggregate nature, whereas, its influence on LITS was negligible. Furthermore, moisture content and heating rate variation did not affect LITS. Moreover, the main factors influencing LITS was stress level and temperature. It was further reported that LITS was observed only during initial heating and did not recover during the subsequent cooling phase. However, temperature higher than the last stage produced additional LITS. According to Khoury et al. (1985a), the main reason for TS is the thermal incompatibilities between cement paste and aggregate. Later on, the experimental results of Khoury et al. (1985a) were modeled by Terro (1998). He proposed 4th and 5th order polynomial functions considering the volume portion and types of aggregates.

Recently, several investigations were devoted to creep behavior of NSC, HSC and HPC at high temperature. Guo and Shi (2011) reported that STC becomes noticeable at a temperature higher than 500 °C. It was observed that the main influencing factors on STC are aggregate type, loading level and its duration. Among others, Hassen and Colina (2006) investigated HPC, Jintao et al. (2013) studied self-compacted concrete, Hu and Dong (2002) investigated HSC with different strength grades and Huismann et al. (2012) studied the effect of PP fibers on HSC.

Creep behavior of concrete at high temperature is of significant importance for fire resistance design and post-fire structural assessment. The amount of creep produced at high temperature in few hours is comparable to several decades creep under normal conditions (Wu et al. 2010). If the creep is neglected in fire safety design, the calculated fire resistance of members is lower than that of actual fire resistance, and the concrete structure may not be safe (Alogla and Kodur 2018). Up to date, traditional types of concretes were extensively studied at high

temperature. However, the creep behavior of RPC is not well known at high temperature and very little information is available. Furthermore, the effect of fibers, which becomes a compulsory constituent due to spalling resistant, is also not understood.

The present research work is aimed at studying STC, FTS and TS behavior of RPC. TS was further investigated at variable loading levels. The effect of PP and hybrid (PP and steel) fibers were evaluated on creeping effects. Experimental results were modeled and fitting equations were proposed. Furthermore, comparative studies were carried out with available literature. This study will be very beneficial for the construction industry as well as academia.

2 Experimentation

2.1 Materials and Mix Proportions

The raw materials used for the preparation of RPC in this study mainly include cement, silica fume, slag, quartz sand, water reducer, steel fiber, PP fiber and polycarboxylic superplasticizer. The physical appearance of raw materials is shown in Fig. 1. The main properties of various constituents are as follows:

2.1.1 Cement

Ordinary Portland cement (P.O 42.5) produced by Heilongjiang Yatai Cement Co., Ltd has been used. The cement quality was as per the Chinese standard

specification (GB175 2007) of common Portland cement. The chemical compositions provided by the manufacturer are listed in Table 1. The cement was used within 1 month after being delivered.

2.1.2 Silica Fume

Silica fume was provided by Jinshi Building Material Company, Gongyi City, Henan Province, China. Its ultra-fine powder is dark grey color. The SiO₂ content was 94%, bulk density was 1700 kg/m³ and the average particle size was 0.1–0.3 μm. The chemical compositions provided by the manufacturer are listed in Table 1.

2.1.3 Slag

The slag produced by Harbin Sanfa New Energy Building Materials Co., Ltd. was used. It's an off-white powder having 2.85 g/cm³ density, 366 m²/kg specific surface area, 81% (7-day) and 103% (28-day) activity index, 93% fluidity ratio and 0.01% chloride ion content. The

Table 1 Chemical composition of cement, silica fume and slag in percentage.

Cementitious materials	SiO ₂	Al ₂ O ₃	Fe ₂ O ₃	CaO	MgO
Cement	21.40	5.45	3.50	64.48	1.46
Silica fume	94.50	0.50	0.45	0.60	0.70
Slag	34.90	14.66	1.36	37.57	9.13



Fig. 1 Raw materials used in the preparation of RPC.

chemical compositions provided by the manufacturer are given in Table 1.

2.1.4 Quartz Sand

The quartz sand produced by Harbin Jinghua Water Treatment Material Co., Ltd. was used. The average nominal sizes of 0.4 mm and 0.2 mm were used with equal ratios. The SiO₂ content in quartz sand was more than 99.6%.

2.1.5 Polycarboxylate Superplasticizer

The polycarboxylate superplasticizer produced by Qingdao Hongxia Concrete Water Reducing Agent Co., Ltd. was used. The PH value was 6–8, water reduction rate was 25–35%, specific gravity was 1.08 ± 0.02 g/cm³ and the solids content was 40%.

2.1.6 Steel Fiber

The straight brass coated steel fiber produced by Changhong Company, Anshan, Liaoning Province was used. The average length was 13 mm, the average diameter was 0.22 mm, the tensile strength was 2850 MPa and elastic modulus was 200 GPa.

2.1.7 Polypropylene Fiber

Polypropylene fiber is a high-strength fiber made of polypropylene as the main raw material. It was provided by Ruixin Fiber Factory, Shijiazhuang, Hebei province. The length was 18–20 mm, average diameter was 45 μm, density was 0.91 g/cm³ and the melting point was 165 °C.

The mix proportion of the co-author (Zheng et al. 2012, 2014) was used, which is summarized in Table 2.

2.2 Specimens Fabrication and Curing

In order to minimise the end effect, prism shape specimens, whose length to width ratio is 3:1, was used. For each type of RPC, a total of 93 prisms of size 70.7 × 70.7 × 220 mm were cast. The results for each test is the arithmetic mean of the two test results. An electronic balance was used for measurements of materials. The mixing was carried out in horizontal pan type mixer which can be adjusted for revolution at different speeds. First of all, dry materials were mixed for 3 min at slow speed of 140 ± 10 revolutions/min. In the next stage, water and liquid superplasticizer were poured into properly mixed dry materials and stirred at high speed of 280 ± 10 revolutions/min for further 5 min. This result in uniform plastic consistency mix. In the last stage, steel and PP fibers were sprinkled

Table 2 Mixture design for HRPC and PRPC.

Constituents	HRPC	PRPC
Ordinary Portland cement (kg/m ³)	815.18	816.42
Silica fume (kg/m ³)	245.31	244.33
Slag (kg/m ³)	120.08	122.16
Quartz coarse sand (kg/m ³)	480.32	490.32
Quartz fine sand (kg/m ³)	480.32	490.32
Water reducer (kg/m ³)	35.40	35.47
PP fiber (kg/m ³)	1.82 (0.2% ^a)	2.73 (0.3% ^a)
Steel fiber (kg/m ³)	157 (2% ^a)	–
Water (kg/m ³)	188.81	189.20
w/b ratio	0.16	0.16

^a Steel and PP fibers are measured as % of RPC volume.

over the course of 2 min and the mix were stirred for total 5 more minutes. The entire mixing process took about 13–15 min. The RPC produced was sufficient workable for construction work. Workability was tested by mortar flow table test method as per the relevant (GB/T-2419 2016). A mini-slump cone was filled with fresh RPC mix on a vibratory table, after the cone is removed and RPC is allowed to spread naturally on the table, then the flow table was dropped 25 times. The average diameter of the spread of RPC shows its workability. The measured flowability of PRPC and HRPC was 180 and 170 mm, respectively. Plastic moulds were oiled before filling in 3 layers. Each layer was consolidated using a vibratory table until oozing slurry appears on the surface of RPC. The top surface was smoothed using a trowel. The moulded specimens were placed for 24 h in laboratory conditions at 25 °C and 70% relative humidity. After 24 h of casting, specimens were removed from the moulds and cured for 72 h in an accelerated steam curing box at 90 °C. Steam curing accelerates the hydration reactions and strength of RPC was increased. After the curing stage, the specimens were stored in laboratory conditions for additional 60 days. Since RPC microstructure is sufficient compact, and melting of PP fibers provide safe passage for releasing vapors pressure during high temperature, still there is fear of fire-induced spalling owing to high amount of moisture content (Zheng et al. 2014). Therefore, specimens were subjected to special heat treatment method (Zheng et al. 2012, 2014). The moisture content of RPC specimens was lowered up to 2.0–3.5% of its initial wet weight, in an oven at 105 °C. The average rate of moisture loss per day was 0.71% to its initial wet weight. In order to protect the specimens from moisture absorption, it were preserved in sealed polyethene bags until the day

of testing. In the preliminary trial experiments, the specimens survived explosive spalling during coupled thermo-mechanical loading. This was a serious concern for this study.

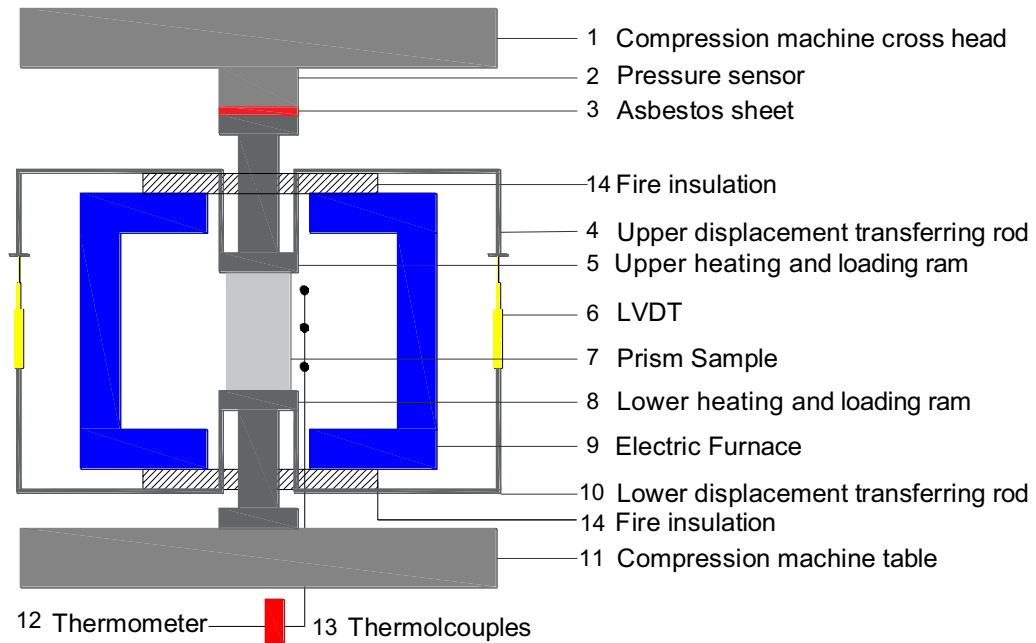
2.3 Testing Approach

2.3.1 Test Equipment

A purpose built furnace with an opening on upper and lower side was used, which allows simultaneous loading during the heating process. The furnace length



a Test-setup for simultaneous heating and loading



b Schematics of test-setup

Fig. 2 Experimental apparatus used in this study.

is 400 mm, external diameter is 400 mm and internal diameter is 250 mm. The test-setup frame and furnace arrangements are shown in Fig. 2a, whereas the schematic representation is shown in Fig. 2b. Two special A321 Nickel-based alloy attachments (platens) were used below and above the specimen in the furnace for simultaneous transmission of load, heating and transferring the deformation of the specimen to the ambient condition. Allow rods were welded to the ends of platens for transmission of deformation outside of the specimens. The exposed part of the alloy platens were wrapped in insulation material, as a safety precaution. The length of alloy platen also works as insulator and protects the testing frame and equipment from extreme heating. Furthermore, ceramic sheets were trapped in between the alloy platens and testing equipment's to protect it from high temperature. A K-type thermocouple, mounted in the middle of the furnace was used to measure and control the heating rate. The furnace can bear a maximum temperature of 1200 °C with a maximum heating rate of 30 °C/min. The specimens surface and centre temperature were recorded by Center-309 thermometer. Load was transmitted by a 100-ton computer controlled universal testing machine (UTM) at a loading rate of 1–5 MPa/s, depending on test requirements. The load was measured by 100-ton pressure sensor, deformation was measured by linear variable differential transformers (LVDT) and a “WS3811-Beijing Wave Spectrum Data-logger” was used for recording the test data. Special steel frame was bolted to the UTM to hold the upper loading platen after failure of the specimen (free fall of upper loading platen) and protects LVDTs and furnace arrangements from damaging.

2.3.2 Measurements of Specimen Temperature

In order to measure the center temperature of the specimen, a thermocouple was installed in the centre core of the specimens during the fabrication process. The surface temperature was measured on the longitudinal midpoint location of the specimen in diametric opposite directions. The surface thermocouples were installed during specimen adjustment process and it was ensured that the thermocouples keep in touch with the specimen during the whole heating process. Temperature variations were recorded at 2 min interval by computer programme of “Center-309” thermometer. WRNK-0101 type thermocouple of two sizes were used. The specimen centre and surface temperature were recorded by 0.5 mm flexible and 3 mm stiff thermocouple, respectively. It can measure up to 1000 °C, with a possible error of ±2.2 °C. STC is measured at target temperatures of 120, 300, 500, 700 and 900 °C. The specimens were heated till centre temperature reaches the target temperature. The FTS was measured till 900 °C, whereas TS was measured till 900 °C or until the specimen failed to stand against the thermo-mechanical load. A heating rate of 5 °C/min was used in this study. The heating-time curves for STC of HRPC and PRPC specimens are shown in Fig. 3a, b, respectively. It is evident that the gradient of surface temperature and centre temperature is lower than the furnace and programme temperature. Therefore to display the creep behaviour against temperature a mean reference temperature of the specimen is required. RILEM recommendations (1997) proposed a relationship for mean temperature of the specimen during transient heating, which will be hereafter called as reference temperature. The formula is given below.

$$T_R = T_S - \frac{1}{3}(T_S - T_C) \tag{1}$$

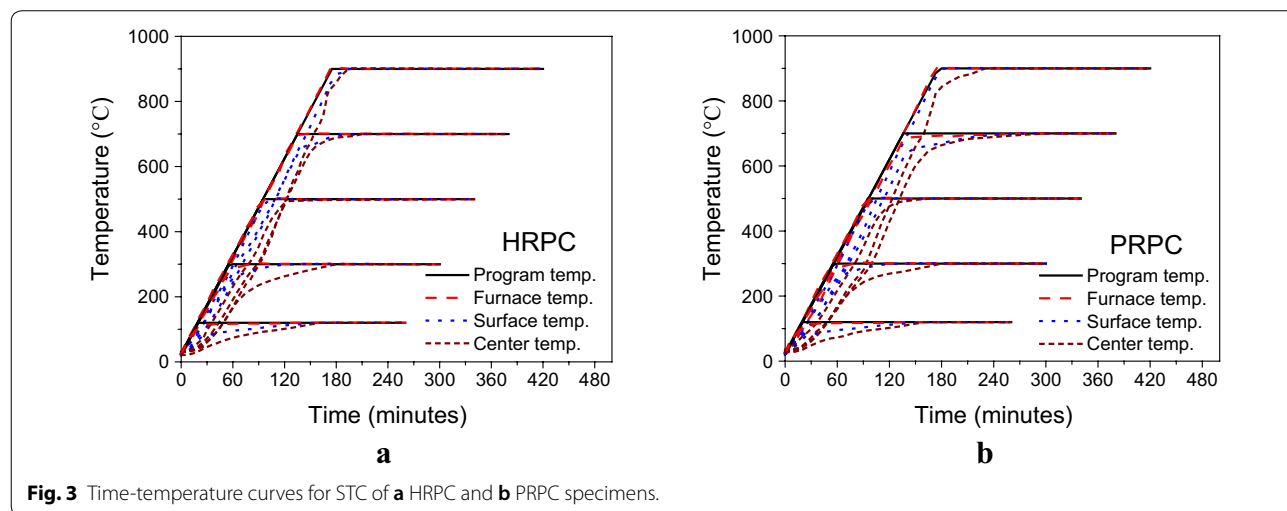


Fig. 3 Time-temperature curves for STC of **a** HRPC and **b** PRPC specimens.

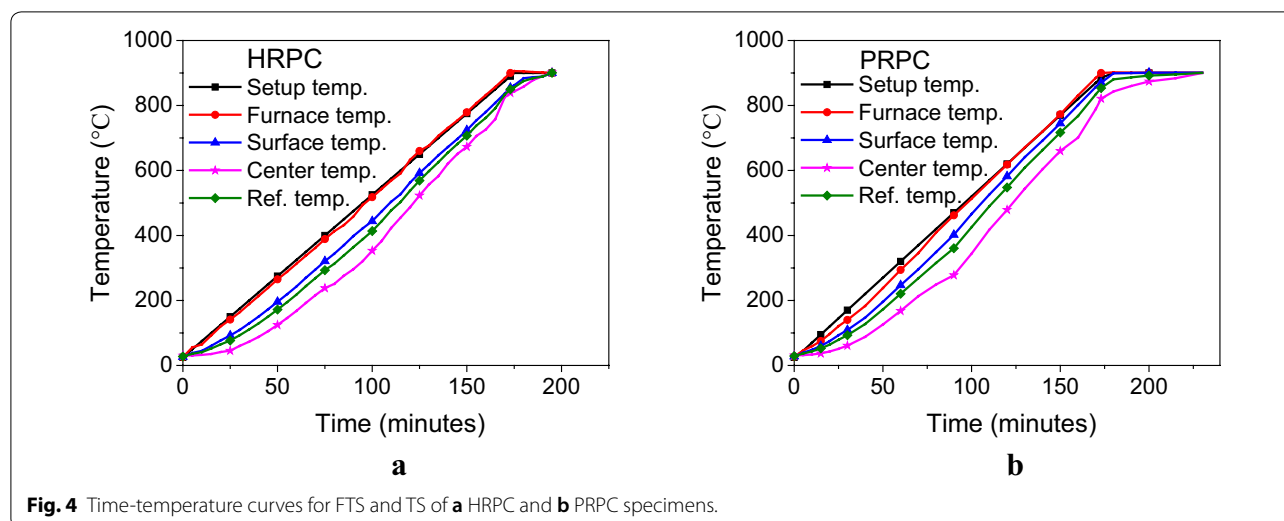


Fig. 4 Time-temperature curves for FTS and TS of **a** HRPC and **b** PRPC specimens.

where T_R is the reference temperature, T_S is the surface temperature and T_C is the specimen center temperature. The reference temperature for HRPC and PRPC are measured for target temperature of 900 °C, which is plotted in Fig. 4a, b, respectively.

2.3.3 Measurements of Specimen Deformation

The specimen deformation has been transferred to the ambient condition by the attached alloy rods. The alloy rods were welded only with those ends of the platens which are connected with the specimen. The special “L” shape alloy rods were welded with the bottom of the top alloy attachment in diametric opposite direction. Similarly, two “U” shape alloy rods of the same material as alloy attachment were welded to the top of the bottom platen. LVDTs were attached with the outside leg of “U” shape bottom rods. Thus the relative deformation of the specimen and loading platen can be measured by averaging the deformation of two LVDTs. Since the deformation was measured on diametric opposite direction, therefore, the eccentric loading and non-rigid loading ram effects are removed. The total deformation includes the deformation of loading platens as well as of RPC specimen. Therefore, the deformation of alloy material was measured separately under the same thermo-mechanical conditions. An alloy sample of same material as of platen and same dimension as the study specimens was used. The temperature of the alloy specimen was assumed to be same as of the furnace. Thus the final deformation was corrected by subtracting the alloy deformation from the total deformation. The thermal expansion measured for alloy specimen was in good agreement with manufacturer theoretical measurements. The creep behaviour of alloy sample was measured under

Table 3 Stress levels of HRPC for STC testing.

Temperature (°C)	Measured in MPa			
	f_c^T	20%	40%	60%
120	130.8	26.2	52.3	78.5
300	119.0	23.8	47.6	71.4
500	99.4	19.9	39.8	59.7
700	64.2	12.8	25.7	38.5
900	36.4	7.3	14.6	21.9

the thermo-mechanical conditions of Fig. 3 and Tables 3 and 4. The details of thermal expansion and creep of alloy specimen has been described in a previous study (Abid et al. 2019a). The measured creep values are in good agreement with the available literature (Brnic et al. 2016) of A321-Nickel based alloy steel. The variation in the expansion of alloy specimen under transient thermal condition at various strength ratios of TS of RPC are so small that only load free thermal expansion and elastic deformation were considered. This is consistent with the calibration of Tao et al. (2013) for the same testing conditions.

2.3.4 Testing Procedure

The high temperature tests for STC, FTS and TS were carried out as per the RILEM recommendations part 8, 6 and 7 (Rilem 1997, 1998, 2000), respectively. The high-temperature creep test setup and procedure used has been described in a previous study (Abid et al. 2019b), but a brief description is provided here, which is summarized in Fig. 5 and explained below.

STC: Specimens were heated to the target temperatures as shown in Fig. 3. The specimens were heated until

Table 4 Stress levels of PRPC for STC testing.

Temperature (°C)	Measured in MPa			
	f_c^T	20%	40%	60%
120	70.4	14.1	28.2	42.3
300	74.2	14.8	29.7	44.5
500	64.6	12.9	25.9	38.8
700	54.8	11.0	21.9	32.
900	29.9	6.0	12.0	18.0

the steady-state thermal condition was achieved, which can be observed by the central thermocouple reading. Load was applied at a quick rate of 5 MPa/s. The load and temperature were kept constant for the test duration of 180 min. The heating rate of 5 °C/min was used in this study. The stress levels (σ/f_c^T) considered were 20, 40

and 60% of high temperature compressive strength at their respective target temperatures of HRPC and PRPC, which is shown in Tables 3 and 4, respectively. Testing procedure for STC is shown in Fig. 5a.

FTS: The thermal expansion of RPC was measured at a heating rate of 5 °C/min up to 900 °C. In order to keep the test arrangements properly aligned and centered, a small pre-load of 0.25 MPa have been sustained during the whole test duration. The load is so small that its effect on expansion properties of RPC is negligible. FTS is plotted as a function of reference temperature as explained in Sect. 2.3.2.

TS: It is not possible up to date to measure the TS of concrete directly. However, an indirect approach has been used, where FTS and elastic strain were subtracted from the total thermal strain (TTS), to measure TS. A heating rate of 5 °C/min was used. The loading rate of 1 MPa/second was used. The strength ratios (σ/f_c)

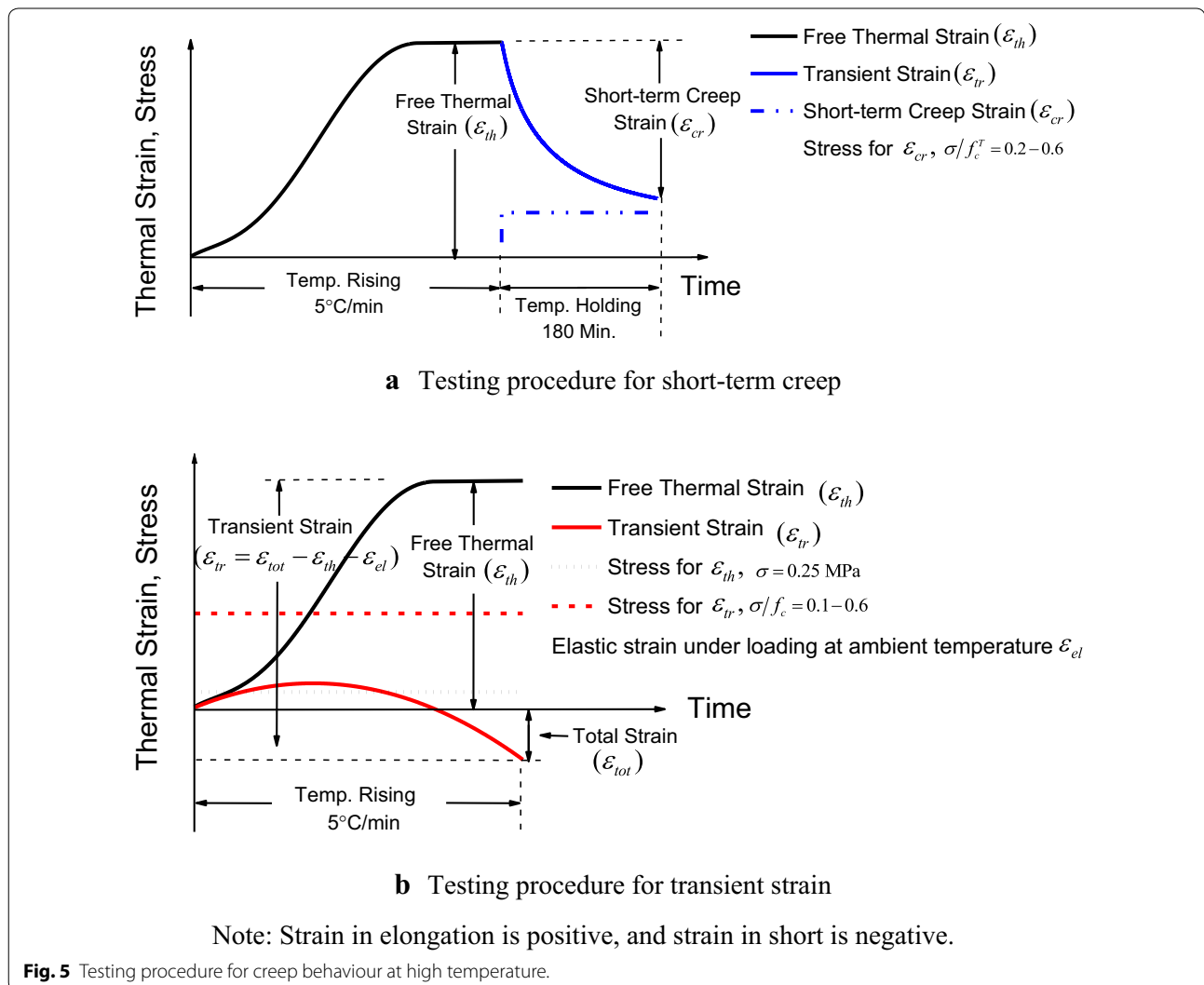


Table 5 Strength ratios for TS testing.

Strength ratios	Measured in MPa	
	HRPC	PRPC
f_c	151.1	97.0
10%	15.1	9.7
20%	30.2	19.4
30%	45.3	29.1
40%	60.4	38.8
50%	75.5	48.5
60%	90.6	58.2

considered for this study were ranging from 10, 20, 30, 40, 50, and 60% ratios of the room temperature compressive strength, as tabulated in Table 5. The strength ratios were applied at ambient temperature and sustained till

target temperature of 900 °C or until the failure of the specimen. TS is also plotted as a function of the reference temperature. Testing procedure for TS is shown in Fig. 5b.

3 Results and Discussions

3.1 Short-Term Creep

The STC of HRPC and PRPC at 20, 40 and 60% stress level to high temperature compressive strength are shown in Figs. 6, 7 and 8, respectively. Generally, the pattern of creep curves is same instead that a rise in stress levels and temperature increases the creep strain. Furthermore, it is evident that the rate of STC was increasing sharply in the first hour, however, after that, it's decreasing slowly. Almost half of the total three hours creep occurred in the first hour, which is also called as primary creep in the literature (Gillen 1981). In low-stress

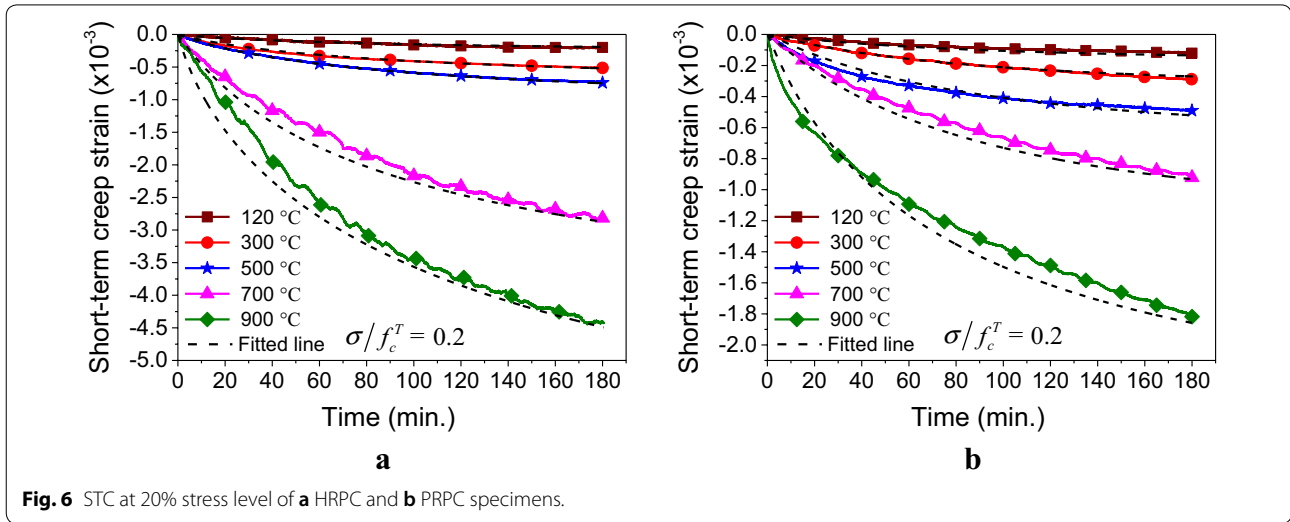


Fig. 6 STC at 20% stress level of **a** HRPC and **b** PRPC specimens.

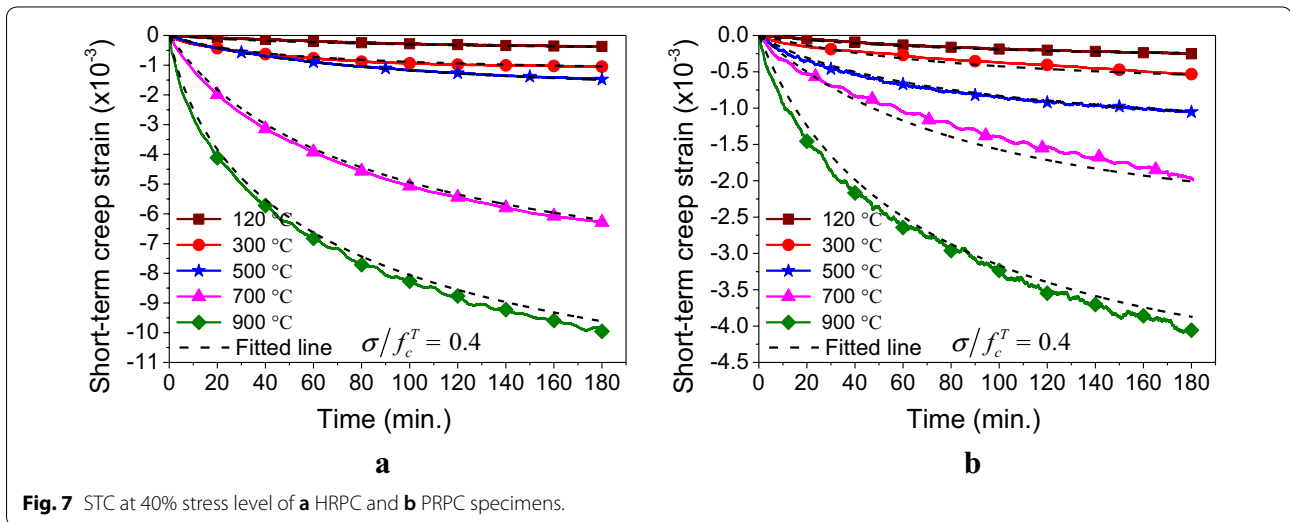
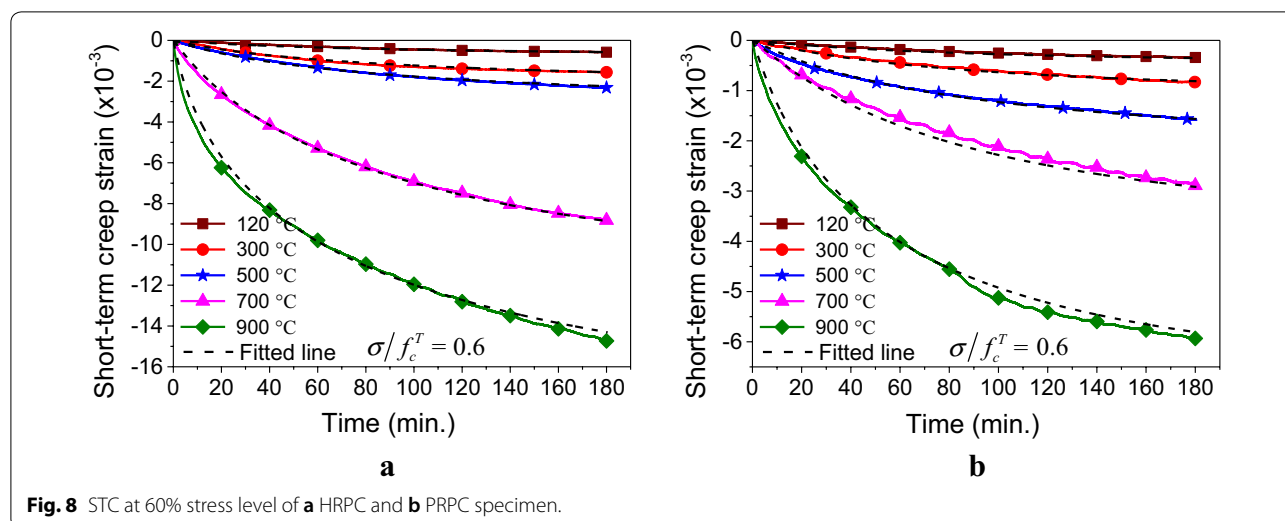


Fig. 7 STC at 40% stress level of **a** HRPC and **b** PRPC specimens.



level ($\sigma/f_c^T = 0.2$), the 3 h STC of HRPC at 20, 300 and 500 °C is 0.20×10^{-3} , 0.51×10^{-3} and 0.74×10^{-3} , respectively. The increase in STC at 300 and 500 °C to 120 °C is 2.51 and 3.62 times. The STC at 700 and 900 °C, becomes noticeable and the measured strain are 2.80×10^{-3} and 4.58×10^{-3} , respectively. This is 13.68 and 22.41 times of their respective strain at 120 °C. Similarly, the STC of PRPC at the 20, 300, 500, 700 and 900 °C are 0.12×10^{-3} , 0.29×10^{-3} , 0.51×10^{-3} , 0.92×10^{-3} and 1.82×10^{-3} , respectively. This is 2.41, 4.28, 7.68 and 15.18 times of strain at 120 °C. At all target temperatures, the STC of PRPC is significantly lower than HRPC. Its mechanism will be explained later.

For the moderate stress levels ($\sigma/f_c^T = 0.4$), the similar trending was observed and the STC was increased almost 1.7–2.2 times of their respective strain at 20% stress level. The markedly high creep strain was observed at 700 and 900 °C. The STC of HRPC and PRPC at 700 °C are 6.29×10^{-3} and 1.99×10^{-3} , respectively. This is 17.46 and 7.89 times of their respective strain at 120 °C. It is also evident that STC of HRPC at 700 °C is 3.15 times greater than PRPC. Furthermore, STC at 900 °C for HRPC and PRPC are 9.98×10^{-3} and 4.04×10^{-3} , respectively. Which is 27.82 and 16.04 times of the 20% stress level strain at 120 °C.

Similarly, in case of the high-stress level ($\sigma/f_c^T = 0.6$), the STC increases significantly especially above 500 °C. The STC of HRPC and PRPC at 700 are 8.82×10^{-3} and 2.88×10^{-3} , respectively. The markedly high strain was observed at 900 °C for HRPC, which is 2.48 times of PRPC strain at the same thermo-mechanical condition.

Overall, at all three stress levels, the STC of HRPC was significantly higher than PRPC. This might be attributed to the presence of steel fibers, which have different

thermal expansion coefficient than the RPC matrix at high temperature (Tai et al. 2011). Furthermore, steel fibers also start to creep at half of its melting temperature (650 °C) (Brnic et al. 2010). Overall the thermal incompatibilities increases between the cementitious paste and steel fibers, which loosen the microstructure and a significant increase in strain was observed (Zheng et al. 2015). It is evident that the micro channels left behind after melting of PP fiber have no prominent contribution in the creep behavior. The gradual rise in STC at increasing temperatures is attributed to the physical and chemical changes take place at elevated temperature. Those are evaporation of capillary and gel water between 100 and 150 °C, chemical bounded water evaporates around 250–300 °C, and CH hydrates changes to calcium oxide around 400–600 °C (Seleem et al. 2011). The markedly high creep strain was observed above 700 and 900 °C, this is due to the high quartz content in RPC mix. Above 570 °C, crystal lattice transformation occurred in quartz and its chemical composition is converted from α to β form, hence resulting in large localized strains at 700 and 900 °C (Abrams 1971). Furthermore, cement paste also transforms from β -C2S to α -C2S around 600 °C (Piasta 1984). The pore radius of cement paste is also increased above 600 °C (Dias et al. 1987). Therefore 600 °C is considered as critical temperature for STC behavior of HRPC and PRPC. According to Dias et al. (1987), the marked increase in STC above 600 °C lies in cement paste. It was further observed that this behavior is similar to “viscous” and “molecular diffusion” type of phenomenon seen in glass, ceramic and metals above a certain critical temperature. Severe cracking was observed in cement paste and steel fibers at 900 °C, which significantly increases the overall compressive creep (Zheng et al. 2013).

The formulas for STC were derived by fitting the experimental data. From the discussion, it is obvious that the most important factors are stress level (σ/f_c^T), temperature (T) and time (t). Therefore, the formulas for STC (ε_{cr}) of HRPC and PRPC is derived based on these parameters as given in Eqs. 2 and 3, respectively.

$$\varepsilon_{cr}(\sigma, T, t) = \begin{cases} -10^{-3} \left(\frac{\sigma}{f_c^T}\right) \left(\frac{t}{t_{total}}\right)^P \left(5.57 - 5.89 \times e^{-2.44 \times 10^{-3}(T-20)}\right), & 120^\circ\text{C} \leq T \leq 500^\circ\text{C} \\ -10^{-3} \left(\frac{\sigma}{f_c^T}\right) \left(\frac{t}{t_{total}}\right)^P \left(65.30 - 98.99 \times e^{-9.89 \times 10^{-4}(T-20)}\right), & 500^\circ\text{C} \leq T \leq 900^\circ\text{C} \end{cases} \quad (2)$$

where,

$$P = \begin{cases} e^{-\left(\frac{t}{140}\right)^{0.4}}, & 120^\circ\text{C} \leq T \leq 700^\circ\text{C} \\ e^{-\left(\frac{t}{40}\right)^{0.2}}, & 700^\circ\text{C} \leq T \leq 900^\circ\text{C} \end{cases} \quad (2b)$$

$$\varepsilon_{cr}(\sigma, T, t) = -0.54 \times 10^{-3} \left(\frac{\sigma}{f_c^T}\right) \left(\frac{t}{t_{total}}\right)^P \times e^{3.28 \times 10^{-3}(T-20)}, \quad 120^\circ\text{C} \leq T \leq 900^\circ\text{C} \quad (3)$$

where,

$$P = \begin{cases} e^{-\left(\frac{t}{80}\right)^{0.4}}, & 120^\circ\text{C} \leq T \leq 700^\circ\text{C} \\ e^{-\left(\frac{t}{80}\right)^{0.3}}, & 700^\circ\text{C} \leq T \leq 900^\circ\text{C} \end{cases} \quad (3b)$$

P is a power function, which is related to time. The fitted lines are also plotted in Figs. 6, 7 and 8 along with experimental data for easy reference.

3.2 Comparison of short-term creep of RPC with NSC and HSC

The STC of RPC has been compared with NSC (Anderberg and Thelandersson 1976) and HSC (Wu et al. 2010) at elevated temperature for 40% stress level, as shown in Figs. 9 and 10. In order to understand the vibrant impor-

tance of high temperature creep, its comparison has also been carried out with the ambient temperature 1 year creep of RPC for 41% stress level, which is $440 \mu\epsilon$ (Graybeal 2005). This amount of strain under the same load ratio can be produced in HRPC and PRPC in 262.8 and 516.4 min at 120°C . Similarly, with the further increasing temperature, this amount of creep can be generated in few minutes which is predicted by the models developed in this study as shown in Table 6. The STC of RPC and its ratio to 1-year ambient temperature creep of RPC is shown in Table 7. It can be seen that STC of RPC is significantly higher and in most severe case it reaches up to 33 times of 1 year ambient temperature creep of RPC. This shows the significance of high-temperature STC which needs to be addressed in the analysis of fire resistant design.

The STC of HRPC is greater than NSC and HSC at all temperature ranges. This might be attributed to the high amount of cementitious materials, quartz aggregate and steel fibers. Cement paste is transformed from anhydrous

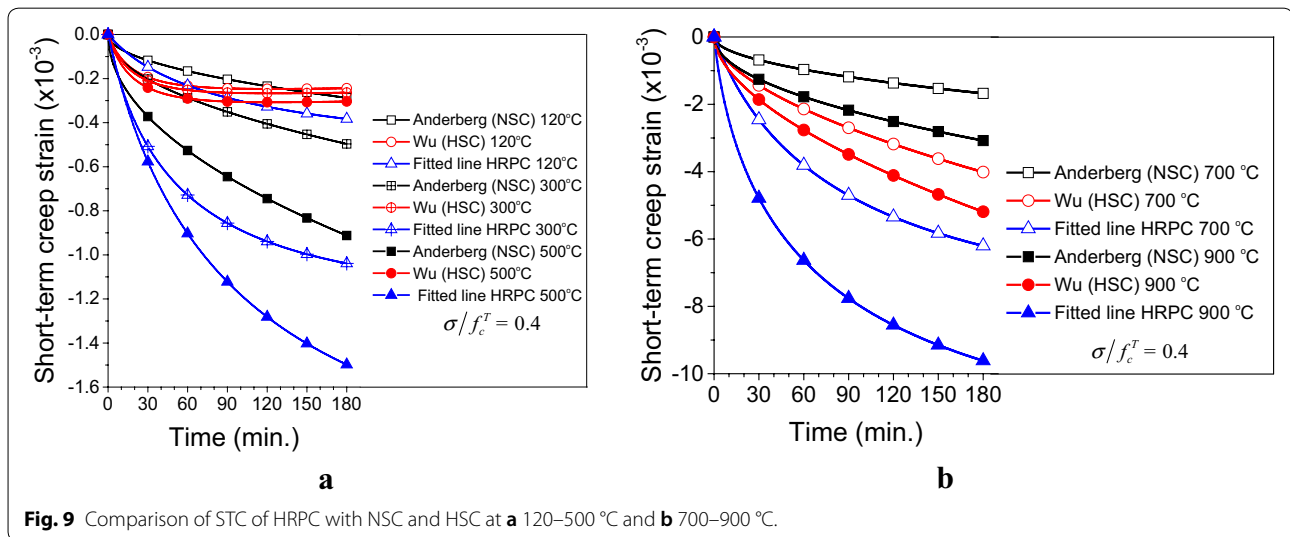


Fig. 9 Comparison of STC of HRPC with NSC and HSC at **a** 120–500 °C and **b** 700–900 °C.

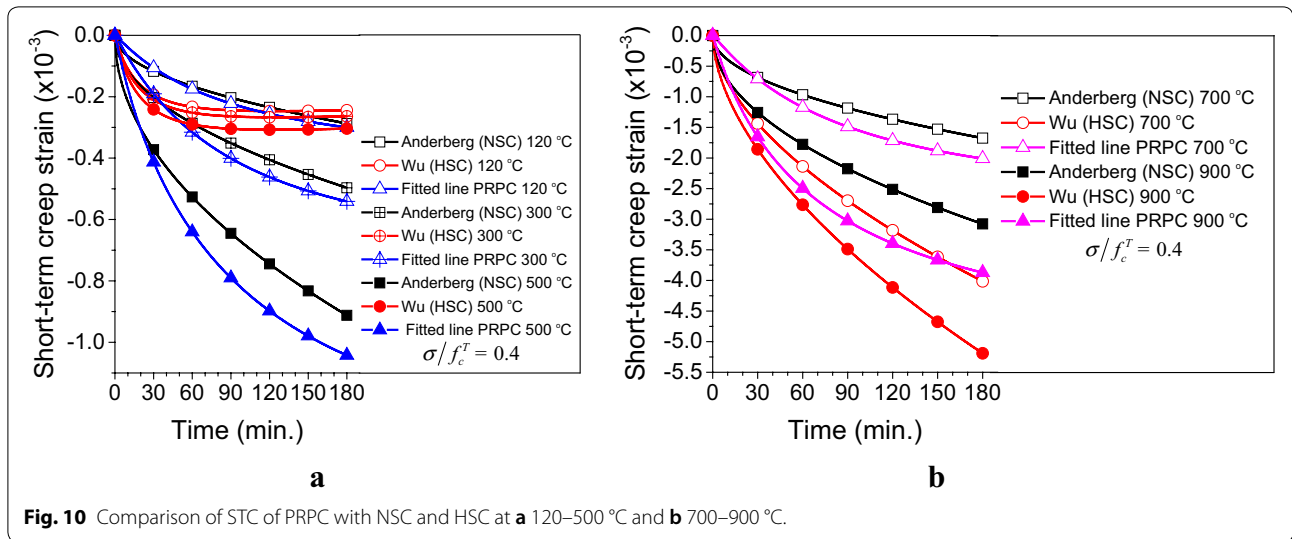


Fig. 10 Comparison of STC of PRPC with NSC and HSC at **a** 120–500 °C and **b** 700–900 °C.

Table 6 Predicted time for STC of RPC equivalent to 1-year ambient temperature creep of RPC.

Temp. (°C)	PRPC (min.)	HRPC (min.)
120	516.4	262.8
300	102.8	23.8
500	31.7	20.2
700	16.8	3.9
900	5.6	1.1

Table 7 STC of RPC and its ratio to 1-year ambient temperature creep of RPC.

Temp. (°C)	Load level (%)	3 h STC ($\times 10^{-3}$)		3 h STC/1-year 20 °C Creep	
		PRPC	HRPC	PRPC	HRPC
120	20	0.12	0.20	0.27	0.47
300		0.29	0.51	0.66	1.17
500		0.49	0.74	1.11	1.68
700		0.92	2.80	2.10	6.36
900		1.82	4.42	4.14	10.05
120	40	0.25	0.36	0.57	0.82
300		0.53	1.05	1.21	2.39
500		1.06	1.47	2.40	3.35
700		1.99	6.29	4.52	14.29
900		4.05	9.98	9.20	22.68
120	60	0.34	0.57	0.78	1.31
300		0.84	1.56	1.90	3.55
500		1.58	2.32	3.59	5.28
700		2.88	8.82	6.54	20.04
900		5.93	14.74	13.47	33.51

β -C2S to α -C2S around 600 °C (Piastra 1984). Furthermore, the “pore radius” of the cement also increases at 600 °C (Dias et al. 1987). Quartz is subjected to volumetric expansion near 570 °C. However, the important role is played by the uneven deformation by steel fibers and cement paste, which enhanced the overall thermal incompatibilities between cement paste, steel fibers and aggregates (Zheng et al. 2015).

On the contrary, the STC of PRPC is similar to NSC (Anderberg and Thelandersson 1976). This might be due to the same siliceous aggregates used in both studies. Similarly, the STC of PRPC performs better than Wu et al. (2010) HSC at a temperature higher than 500 °C. Unexpectedly, the STC of HSC is quite low below 500 °C, no explanation is given for this phenomenon. From the comparison, it is also evident that STC increases with increasing strength. The same was also reported by Xing et al. (2011) for different strength grades of HSC.

3.3 Free Thermal Strain

The results of FTS of HRPC and PRPC are summarized in Fig. 11. The overall response of FTS can be characterized in three distinct temperature ranges. The initial slow expansion stage from room temperature to 250 °C, at the end of this stage, PRPC stagnates from HRPC. The middle stage, where a sharp increase in expansion was observed. The final stage where both HRPC and PRPC becomes constant and no further expansion was observed. The stagnation of PRPC about 200–250 °C is because of evaporation process (Huisman et al. 2012). PP fiber melt nearly 200 °C, left micro-channels, where the free, capillary and chemically bounded water starts to evaporate quickly. The same stagnation phenomenon was also observed by Wu et al. (2010)

and Huismann et al. (2012) for PP fiber reinforced HSC. The stagnation phenomenon in HRPC was not observed because these samples were dried for more time as compared to PRPC specimens. The additional drying process removed most of the free water and the evaporation process was not prominent. The steel fibers also restrict the stagnation process because its expansion rate differs from RPC matrix at high temperature (Tai et al. 2011).

The expansion rate in the initial stage was quite low because of simultaneous expansion of aggregates and cement paste and shrinkage due to moisture loss. Overall, both these reactions compensate each other and the resultant expansion rate was reduced (Guo and Shi 2011). The FTS of HRPC and PRPC measured at 150 °C are 0.26×10^{-3} and 0.24×10^{-3} , respectively. The expansion rate increases above 250 °C, and the HRPC and PRPC reaches its maximum value of 15.17×10^{-3} and 15.34×10^{-3} at 680 °C and 705 °C, respectively. The expansion rate was too sharp in the range of 250–700 because of various changes that take place at high temperature. Those

are the conversion of calcium hydroxide to calcium oxide, breakage of CH and C–S–H hydrates at 400–600 °C, breakage of the interfacial transition zone and the most important is the phase changes of quartz aggregate from α to β form at nearly 573 °C (Khoury et al. 2007; Fu et al. 2004). The expansion rate ceased down at the last heating stage (above 680 °C) and FTS remain unchanged till the target temperature. The expansion strain maybe obstructed because the crystals of mineral components change within the aggregates and total internal damages in concrete were accumulated already (Guo and Shi 2011). Overall, the expansion of HRPC was slightly higher than PRPC because of uneven expansion of steel fibers from the RPC matrix. This additional expansion accelerated the overall FTS of HRPC and a slight increase was observed above 250 °C (Zheng et al. 2015).

The experimental results were fitted by fifth order polynomial equations, and formulas are derived for FTS (ϵ_{cr}) as a function of temperature (T). The formulas for HRPC are expressed as;

$$\epsilon_{th} = \begin{cases} A_0 + A_1T + A_2T^2 + A_3T^3 + A_4T^4 + A_5T^5, & 20^\circ\text{C} \leq T \leq 680^\circ\text{C} \\ 15.17 \times 10^{-3}, & 680^\circ\text{C} < T \leq 900^\circ\text{C} \end{cases} \quad (4)$$

And the formulas for PRPC are given as;

$$\epsilon_{th} = \begin{cases} B_0 + B_1T + B_2T^2 + B_3T^3 + B_4T^4 + B_5T^5, & 20^\circ\text{C} \leq T \leq 705^\circ\text{C} \\ 15.34 \times 10^{-3}, & 705^\circ\text{C} < T \leq 900^\circ\text{C} \end{cases} \quad (5)$$

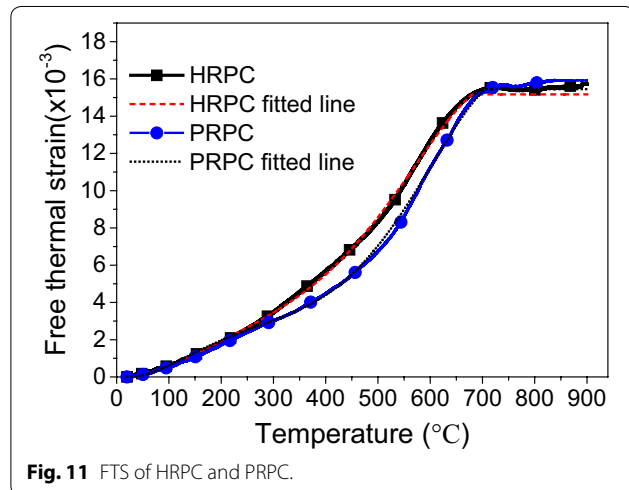


Fig. 11 FTS of HRPC and PRPC.

where,

$$\begin{aligned} A_0 &= 4.22 \times 10^{-5} & \text{and } B_0 &= 1.1 \times 10^{-4} \\ A_1 &= -4.49 \times 10^{-6} & B_1 &= -9.31 \times 10^{-6} \\ A_2 &= 1.49 \times 10^{-7} & B_2 &= 2.22 \times 10^{-7} \\ A_3 &= -5.86 \times 10^{-10} & B_3 &= -9.46 \times 10^{-10} \\ A_4 &= 1.09 \times 10^{-12} & B_4 &= 1.68 \times 10^{-12} \\ A_5 &= -6.89 \times 10^{-16} & B_5 &= -9.96 \times 10^{-16} \end{aligned}$$

The fitted lines are plotted along with their experimental results as shown in Fig. 11.

3.4 Comparison of Free Thermal Strain of RPC with NSC and HSC

The FTS of HRPC and PRPC are compared with NSC (Guo and Shi 2011), HSC (Wu et al. 2010; Kodur and Khaliq 2010) and design codes (Eurocode 1995; ASCE 1992) at high temperature, as shown in Fig. 12. The expansion of concrete is being influenced by aggregate type, moisture content, cement type and heating rate (ASCE 1992; Bazant and Chern 1987). Therefore different types of concretes will have different thermal expansion.

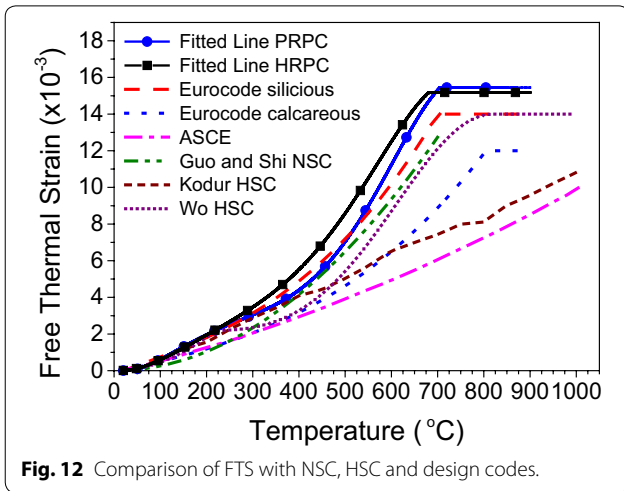


Fig. 12 Comparison of FTS with NSC, HSC and design codes.

The PRPC have similar trending as of that Eurocode siliceous concrete model (Eurocode 1995). However, HRPC observed a steeper gradient due to uneven expansion of steel fibers (Tai et al. 2011). The FTS of Wu et al. (2010) HSC and Guo and Shi (2011) NSC are also higher than Kodur and Khaliq (2010) HSC, Eurocode calcareous (1995) and ASCE models (1992). The detailed explanation of each case might be different, however, the different types of aggregates used in their concretes are one of the important reason behind this variation.

3.5 Transient Strain at Constant Loading

Up to date, no experimental testing technique has been developed to measure TS of concrete directly. However, since its first existence by Johansen and Best, cited by Khoury et al. (1985b), its measured indirectly by subtracting FTS and elastic strain from TTS. This is an important part of TTS, which is also called as mechanical

strain by some of the researchers (Huisman et al. 2012). The LITS can further be separated into transient thermal creep, drying creep, shrinkage strain and elastic strain. Transitional thermal creep and drying creep makes the TS. It is the main component of LITS and its value is far greater than the STC, FTS and stain induced by the instantaneous stresses, as can be seen in Fig. 13a, b, for HRPC and PRPC, respectively. TS is calculated by the following equation (Rilem 1998; Khoury et al. 1985a, b; Schneider 1988).

$$\varepsilon_{tr}(T, \sigma) = \varepsilon_{tot}(T, \sigma) - \varepsilon_{th}(T, \sigma = 0) - \varepsilon_{el}(T, \sigma) - \varepsilon_{sh}(T, \sigma = 0) \tag{6}$$

where ε_{el} is elastic strain and ε_{sh} is shrinkage strain. The shrinkage strain component can be coupled with FTS (Rilem 1997; Khoury et al. 1985a; Schneider 1988; Thienel and Rostasy 1996), therefore the Eq. 5 will be simplified as;

$$\varepsilon_{tr}(T, \sigma) = \varepsilon_{tot}(T, \sigma) - \varepsilon_{th}(T, \sigma = 0) - \varepsilon_{el}(T, \sigma) \tag{7}$$

TS for HRPC and PRPC is calculated from Eq. 7 and is plotted as function of reference temperature, which is shown in Fig. 13a, b, respectively. It is evident that higher strength ratios and rising temperature increasing TS. The response of TS over the temperature span can be divided into three distant stages. Initially, the change in TS was negligible up to 250 °C. This might be due to the absence of free water, which was removed during the pre-heating procedure as explained in Sect. 2.2. Therefore, the drying creep and transitional thermal creep were inexistent and overall, no prominent change was observed in this range (Khoury et al. 1985a). The middle stage probably starts above 250 °C, however, its last ending phase from where very large compressive strain originates, depends on the strength ratios.

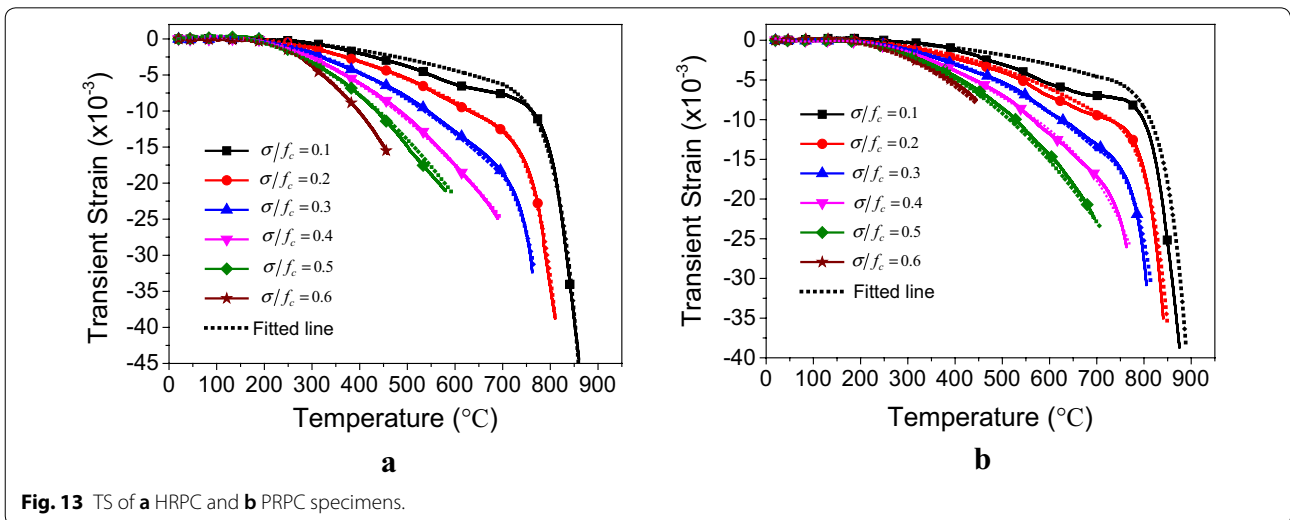


Fig. 13 TS of a HRPC and b PRPC specimens.

Approximately, 700 °C might be the end temperature for the middle stage where a gradual increase in TS was observed. Furthermore, TS increasing with higher strength ratios. For instance, the TS of HRPC at 500 °C and strength ratios of 0.3, 0.4 and 0.5 are -8.08×10^{-3} , -10.86×10^{-3} (1.35 times of $0.3\varepsilon_{tr}$) and -14.90×10^{-3} (1.85 times of $0.3\varepsilon_{tr}$), respectively. Similarly, the TS of PRPC at above-mentioned conditions are -5.9×10^{-3} , -6.92×10^{-3} (1.17 times of $0.3\varepsilon_{tr}$) and -8.52×10^{-3} (1.44 times of $0.3\varepsilon_{tr}$), respectively. This is evident that higher strength ratio increases TS. The quartz transformation has no prominent influence on TS. It is evident from the gradient of TS curves just before and after 573 °C, which is a critical temperature stage for quartz transformation. The same behaviour was also observed by Khoury et al. (1985a). In the last stage, just before the failure of the specimen, a sharp descending strain was observed. This was due to the severe cracking, as the specimen reaches its ultimate compressive strength at high temperature.

TS possibly originated due to the irrecoverable physical and chemical changes in the concrete during high temperature, that is dehydration of C-S-H gel and changes in

porosity of the microstructure (Hassen and Colina 2006). Furthermore, the conversion of portlandite Ca(OH)_2 into calcium oxide changes the porous network. Overall, during coupled thermo-mechanical loading, the porous volume increases and the stiffness decreases. This results in remarkable compressive strain (Tao et al. 2013).

The TS of HRPC has been compared with PRPC at 20, 40 and 60% strength ratios, as shown in Fig. 14. It is evident that the TS of HRPC is higher than PRPC. For example, the TS at 60% strength ratio of PRPC is equal to 40% TS of HRPC. This difference is due to the presence of steel fibers in HRPC, which expands unevenly than of concrete paste and also starts to creep at high temperature. Thus, the incompatibilities between cement paste and steel fibers increase the porous network and decrease the stiffness of microstructure. This results in higher TS at high temperature.

From the discussion, it is concluded that the most important factors for TS (ε_{tr}) are strength ratios (σ/f_c) and temperature (T). Therefore, TS is modeled as a function of strength ratios and temperature by regression analysis. The derived formulas for HRPC and PRPC are shown in Eqs. 8 and 9, respectively.

$$\varepsilon_{tr} = \begin{cases} \frac{\sigma}{f_c}(-6.51 \times 10^{-4} + 3.16 \times 10^{-5}T - 1.72 \times 10^{-7}T^2 - 9.55 \times 10^{-14}T^3), & 120^\circ\text{C} \leq T \leq 700^\circ\text{C} \\ \frac{\sigma}{f_c}(-49.66 \times 10^{-3} - 6.63 \times 10^{-9} \times e^{0.0208 \times T}), & 700^\circ\text{C} \leq T \leq 900^\circ\text{C} \end{cases} \quad (8)$$

$$\varepsilon_{tr} = \begin{cases} \frac{\sigma}{f_c}(-8.17 \times 10^{-4} + 1.92 \times 10^{-5}T - 8.23 \times 10^{-8}T^2 - 5.27 \times 10^{-11}T^3), & 120^\circ\text{C} \leq T \leq 700^\circ\text{C} \\ \frac{\sigma}{f_c}(-40.88 \times 10^{-3} - 2.92 \times 10^{-10} \times e^{0.0235 \times T}), & 700^\circ\text{C} \leq T \leq 900^\circ\text{C} \end{cases} \quad (9)$$

The fitting equations are plotted along with the experimental data in Fig. 17, for easy reference.

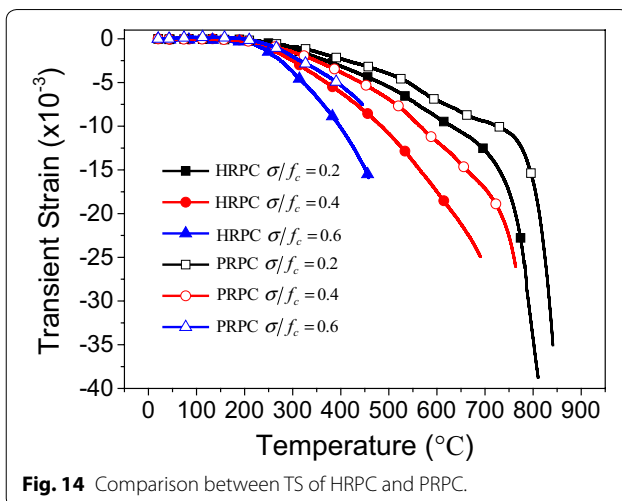
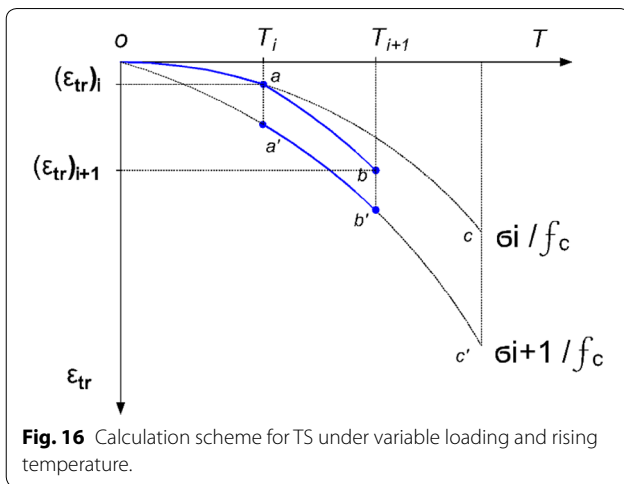
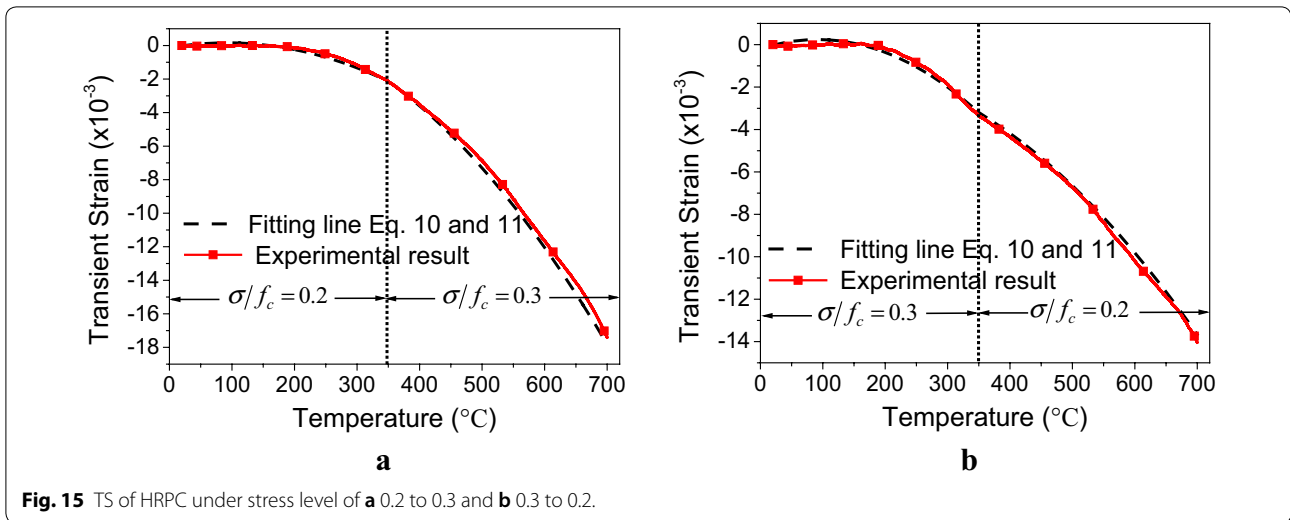


Fig. 14 Comparison between TS of HRPC and PRPC.

3.6 Transient Strain at Variable Loading

The structural fire is a complex phenomenon, where the temperature and stress level is changing. Therefore, the effect of variable loading on TS behavior was studied for HRPC. TS under progressive increase from 20% to 30% strength ratios is shown in Fig. 15a. Whereas, when the strength ratio was decreased from 30 to 20%, the TS obtained as shown in Fig. 15b. It is evident that the gradient of TS increases prominently when the strength ratio increases. Similarly, by decreasing the strength ratio no obvious increase in the rate of transient strain was observed.

The TS under variable stress can be modeled by incremental method (Guo and Shi 2011). A schematic diagram of the variable TS has been shown in Fig. 16.

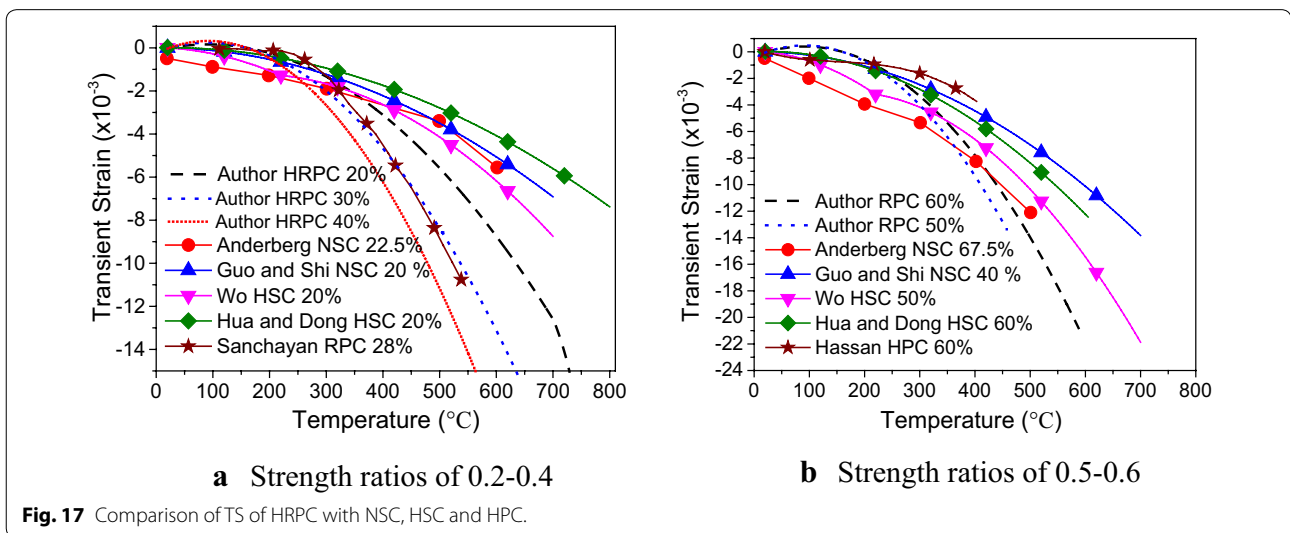


The TS at strength ratio σ_i/f_c up to temperature T_i is $(\epsilon_{tr})_i$, plotted by “oac” line in Fig. 16. Similarly, the TS at strength ratio σ_{i+1}/f_c up to temperature T_{i+1} is $(\epsilon_{tr})_{i+1}$, plotted by “oa'b'” line. It is assumed that path “ab” is equal to “a'b'”. The TS under strength ratio σ_{i+1}/f_c and temperature T_{i+1} can be calculated by the following equations.

$$(\epsilon_{tr})_{i+1} = (\epsilon_{tr})_i + \Delta(\epsilon_{tr})_i \tag{10}$$

where,

$$\Delta(\epsilon_{tr})_i = \epsilon_{tr} \left(\frac{\sigma_{i+1}}{f_c}, T_{i+1} \right) - \left(\epsilon_{tr} \frac{\sigma_{i+1}}{f_c}, T_i \right) \tag{11}$$



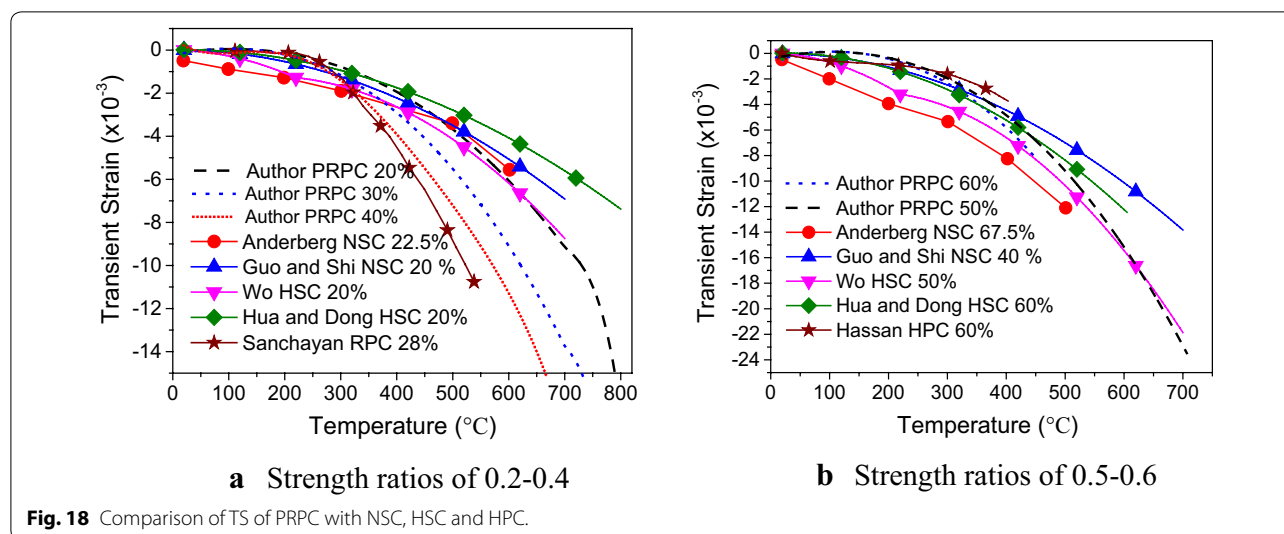


Fig. 18 Comparison of TS of PRPC with NSC, HSC and HPC.

The TS under variable stresses were calculated based on Eq. 10 and 11, and the results were plotted in Fig. 15 along with experimental data. The model result compares well with the experimental data.

3.7 Comparison of Transient Strain of RPC with NSC and HSC

The TS of HRPC and PRPC has been compared with available models of NSC (Anderberg and Thelandersson 1976; Guo and Shi 2011), HSC (Wu et al. 2010; Hu and Dong 2002) and HPC (Hassen and Colina 2006) in Figs. 17 and 18, respectively. The TS of concrete depends on the type of aggregate, type of cement, moisture content, strength and age of concrete (Schneider 1988). Based on these influencing factors, different types of concretes will have different TS behavior. RPC being rich in cementitious materials, and with siliceous aggregates, is more susceptible to high TS. TS of PRPC and HRPC is lower in the NSC and HSC up to 250 °C. This might be due to initial heat treatment method, which removed free moisture content and ultimately shrinkage strain and dry creep were reduced (Khoury et al. 1985a). Above 250 °C, HRPC and PRPC showed a large TS than NSC and HSC. This might be due to the siliceous aggregates being used in RPC. The TS of Anderberg and Thelandersson (1976) NSC is higher than Guo and Shi (2011) NSC. This might be due to the use of siliceous aggregates being used by the former. TS measured by Sanchayan and Foster (2016) for RPC at 28% stress level is similar to 30% stress level of HRPC. However, higher than TS of PRPC at 40% stress level. This high TS might be due to the presence of steel fibers in the former.

4 Conclusions

The main conclusions drawn from experimental results are summarized as follows:

- In general, an increase in STC was observed with higher stress levels and rising temperature. The STC originates quickly at the start of the test, and almost half of the total creep developed within 1 h heating. However, its rates ceased down after the first hour. The STC developed below 500 °C, was low for both types of RPC, while above the transition stage of quartz aggregate, the evolution of STC was pronounced. In most severe case 3 h STC reaches up to 33 times of 1 year ambient temperature creep. STC needs to be addressed in fire safety design.
- The STC of HRPC was significantly higher than PRPC. This can be attributed to the presence of steel fibers, which have different thermal expansion coefficient than the RPC matrix at high temperature. Furthermore, steel fibers also start to creep at half of its melting temperature (650 °C). Overall, the thermal incompatibilities increase between the cementitious paste and steel fibers, which damaged the microstructure and a significant increase in strain was obtained. The micro-channels left after melting of PP fiber have no prominent contribution in the STC behavior.
- The STC of HRPC is greater than NSC and HSC. This can be attributed to the high amount of cementitious materials, quartz aggregate and steel fibers being used in HRPC. On the other hand, the STC of PRPC is lower than HSC at high temperature. The STC of PRPC is similar as siliceous aggregate NSC but higher than the carbonaceous aggregate NSC.

- The PRPC has similar evolution of FTS as that of Eurocode siliceous concrete model. However, HRPC observed a steeper gradient due to uneven expansion of steel fibers and RPC matrix.
- The higher stress levels and rising temperature increases TS. The gradient of TS increases prominently when the strength ratio increases. Whereas, by decreasing the strength ratio, there is no obvious increase in the rate of TS. Furthermore, TS of HRPC is higher than PRPC. This can be attributed again due to the uneven expansion between the steel fibers and RPC matrix. Further, TS of RPC is lower than NSC and HSC below 250 °C. However, above 250 °C, both HRPC and PRPC showed higher TS than NSC and HSC. This is due to the siliceous aggregates being used in RPC.
- Constitutive relationships are proposed for creep behavior of HRPC and PRPC, which will be used as input data in numerical models for fire resistance calculations.

Abbreviations

f_c : prism compressive strength at ambient temperature; f_c^T : prism compressive strength at high temperature; $\frac{f_c^T}{f_c}$: strength ratios with respect to ambient temperature compressive strength; $\frac{\sigma}{f_c^T}$: strength ratios with respect to high temperature compressive strength. This is also called as stress level in the paper; ε_{cr} : short-term creep at high temperature (STC); ε_{el} : elastic strain under loading at ambient temperature; ε_{th} : free thermal strain at high temperature (FTS); ε_{tr} : transient strain at high temperature (TS); TTS: total thermal strain; LITS: load-induced thermal strain.

Acknowledgments

The investigation presented in this paper is supported by the National Natural Science Foundation of China (Nos. 51578184, 51408167), and the postdoctoral scientific research developmental fund of Heilongjiang Province (No. LBH-Q15058), the Natural Science Foundation of Heilongjiang Province (QC2017058) and Foundation of Key Laboratory of Structures Dynamic Behavior and Control (Ministry of Education) in Harbin Institute of Technology (30620180341).

Authors' contributions

XH conceived and designed the experiments; MA and XH performed the experiments. All the authors analyzed the data and contributed to writing the paper. All authors read and approved the final manuscript.

Funding

The investigation presented in this paper is supported by the National Natural Science Foundation of China (Nos. 51578184, 51408167), and the postdoctoral scientific research developmental fund of Heilongjiang Province (No. LBH-Q15058), the Natural Science Foundation of Heilongjiang Province (QC2017058) and Foundation of Key Laboratory of Structures Dynamic Behavior and Control (Ministry of Education) in Harbin Institute of Technology (30620180341).

Availability of data and materials

The data and material sets supporting the results of this article are included within the article.

Ethics approval and consent to participate

The manuscript has not been published previously, that it is not under consideration for publication elsewhere, that its publication is approved by

all authors and tacitly or explicitly by the responsible authorities where the work was carried out, and that, if accepted, it will not be published elsewhere in the same form, in English or in any other language, including electronically without the written consent of the copyright-holder.

Consent for publication

Not applicable.

Competing interests

The authors declare that they have no competing interests.

Author details

¹ Key Lab of Structures Dynamic Behavior and Control of the Ministry of Education, Harbin Institute of Technology, Harbin 150090, China. ² Key Lab of the Smart Prevention and Mitigation of Civil Engineering Disasters of the Ministry of Industry and Information Technology, Harbin Institute of Technology, Harbin 150090, China. ³ College of Aerospace and Civil Engineering, Harbin Engineering University, Harbin 150001, China. ⁴ Civil Engineering Department, College of Engineering, King Saud University, Riyadh 11421, Saudi Arabia.

Received: 27 June 2018 Accepted: 5 July 2019

Published online: 22 August 2019

References

- Abid, M., Hou, X., Zheng, W., & Hussain, R. R. (2017). High temperature and residual properties of reactive powder concrete—a review. *Construction and Building Materials*, 147, 339–351.
- Abid, M., Hou, X., Zheng, W., & Hussain, R. R. (2019a). Effect of fibers on high-temperature mechanical behavior and microstructure of reactive powder concrete. *Materials*, 12(2), 329.
- Abid, M., Hou, X., Zheng, W., Hussain, R. R., Cao, S., & Lv, Z. (2019b). Creep behavior of steel fiber reinforced reactive powder concrete at high temperature. *Construction and Building Materials*, 205, 321–331.
- Abrams, M. S. (1971). Compressive strength of concrete at temperatures to 1600F. *Special Publication*, 25, 33–58.
- Alogla, S., & Kodur, V. (2018). Quantifying transient creep effects on fire response of reinforced concrete columns. *Engineering Structures*, 174, 885–895.
- American Society of Civil Engineers. (1992). *Structural fire protection* (p. 1992). New York: Committee on Fire Protection, Structural Division, ASCE.
- Anderberg, Y., & Thelandersson, S. (1976). Stress and deformation characteristics of concrete at high temperatures. 2. Experimental investigation and material behaviour model. *Bulletin of Division of Structural Mechanics and Concrete Construction*, 54, 2.
- Bamonte, P., & Gambarova, P. G. (2009). Thermal and mechanical properties at high temperature of a very high-strength durable concrete. *Journal of Materials in Civil Engineering*, 22, 545–555.
- Bažant, Z. P., & Chern, J.-C. (1987). Stress-induced thermal and shrinkage strains in concrete. *Journal of Engineering Mechanics*, 113, 1493–1511.
- Bierwagen, D., & Abu-Hawash, A. (2005). Ultra high performance concrete highway bridge. In Proceedings of the 2005 Mid-continent transportation research symposium, Ames, Iowa. pp 1–14.
- British Standard Institute. (1995). Eurocode 2: Design of concrete structures—part 1.2: General rules—structural fire design. BS EN. 1992-1-2:2004.
- Bronic, J., Niu, J.-T., Turkalj, G., Canadija, M., & Lanc, D. (2010). Experimental determination of mechanical properties and short-time creep of AISI 304 stainless steel at elevated temperatures. *International Journal of Minerals, Metallurgy, and Materials*, 17, 39–45.
- Bronic, J., Turkalj, G., Canadija, M., Lanc, D., Krcanski, S., Bronic, M., et al. (2016). Mechanical properties, short time creep, and fatigue of an austenitic steel. *Materials*, 9, 298.
- Cheyrezy, M., Maret, V., & Frouin, L. (1995). Microstructural analysis of RPC (reactive powder concrete). *Cement and Concrete Research*, 25, 1491–1500.
- Dias, W., Khoury, G., & Sullivan, P. (1987). Basic creep of unsealed hardened cement paste at temperatures between 20 °C and 725 °C. *Magazine of concrete research*, 39, 93–101.

- Fu, Y.-F., Wong, Y.-L., Poon, C.-S., Tang, C.-A., & Lin, P. (2004). Experimental study of micro/macro crack development and stress-strain relations of cement-based composite materials at elevated temperatures. *Cement and Concrete Research*, 34, 789–797.
- GB175. (2007). *Standard for ordinary portland cement*. Beijing: Chinese Standard Publishing. (In Chinese).
- GB/T-2419. (2016). *Test method for fluidity of cement mortar*. Beijing: Chinese Standard Publishing. (In Chinese).
- Gillen, M. (1981). Short-term creep of concrete at elevated temperatures. *Fire and Materials*, 5, 142–148.
- Graybeal, B. (2004). *Fabrication of an optimized UHPC bridge*. Atlanta: PCI National Bridge Conference.
- Graybeal, B. (2005). *Characterization of the behavior of ultra-high performance concrete*. Ph.D. thesis, University of Maryland, USA.
- Guo, Z., & Shi, X. (2011). *Experiment and calculation of reinforced concrete at elevated temperatures*. New York: Elsevier.
- Hassen, S., & Colina, H. (2006). Transient thermal creep of concrete in accidental conditions at temperatures up to 400 °C. *Magazine of Concrete Research*, 58, 201–208.
- Hou, X., Cao, S., Rong, Q., Zheng, W., & Li, G. (2018). Effects of steel fiber and strain rate on the dynamic compressive stress-strain relationship in reactive powder concrete. *Construction and Building Materials*, 170, 570–581.
- Hou, X., Ren, P., Rong, Q., Zheng, W., & Zhan, Y. (2019a). Effect of fire insulation on fire resistance of hybrid-fiber reinforced reactive powder concrete beams. *Composite Structures*, 209, 219–232.
- Hou, X., Ren, P., Rong, Q., Zheng, W., & Zhan, Y. (2019b). Comparative fire behavior of reinforced RPC and NSC simply supported beams. *Engineering Structures*, 185(2019), 122–140.
- Hu, H., & Dong, Y. (2002). Experimental Research on the Transient Thermal Strain of High Strength Concrete at Elevated Temperature. *Journal of Building Structures*, 4, 006.
- Huisman, S., Weise, F., Meng, B., & Schneider, U. (2012). Transient strain of high strength concrete at elevated temperatures and the impact of polypropylene fibers. *Materials and Structures*, 45, 793–801.
- Khoury, G., Anderberg, Y., Both, K., Fellingner, J., Høj, N., & Majorana, C. (2007). *Fib bulletin 38: Fire design of concrete structures—materials, structures and modelling, state-of-the-art report*. Lausanne, Switzerland: Federation Internationale du Beton.
- Khoury, G. A., Grainger, B. N., & Sullivan, P. J. (1985a). Strain of concrete during first heating to 600 °C under load. *Magazine of Concrete Research*, 37, 195–215.
- Khoury, G. A., Grainger, B. N., & Sullivan, P. J. (1985b). Transient thermal strain of concrete: Literature review, conditions within specimen and behaviour of individual constituents. *Magazine of Concrete Research*, 37, 131–144.
- Kodur, V., & Khaliq, W. (2010). Effect of temperature on thermal properties of different types of high-strength concrete. *Journal of Materials in Civil Engineering*, 23, 793–801.
- Piasta, J. (1984). Heat deformations of cement paste phases and the micro-structure of cement paste. *Matériaux et Construction*, 17, 415–420.
- Richard, P., & Cheyrezy, M. H. (1994). Reactive powder concretes with high ductility and 200–800 MPa compressive strength. *Special Publication*, 144, 507–518.
- Richard, P., & Cheyrezy, M. (1995). Composition of reactive powder concretes. *Cement and Concrete Research*, 25, 1501–1511.
- Rilem, T. (1997). 129-MHT. Test method for mechanical properties of concrete at high temperatures: Part 6—thermal strain. *Materials and Structures*, 30, 17–21.
- Rilem, T. (1998). 129-MHT. Test methods for mechanical properties of concrete at high temperatures. Recommendations: Part 7: Transient creep for service and accident conditions. *Materials and Structures*, 31, 290.
- Rilem, T. (2000). 129-MHT. Test methods for mechanical properties of concrete at high temperatures: Part 8 steady-state creep and creep recovery for service and accident conditions. *Materials and Structures*, 33, 6–13.
- Sanchayan, S., & Foster, S. J. (2016). High temperature behaviour of hybrid steel-PVA fibre reinforced reactive powder concrete. *Materials and Structures*, 49, 769–782.
- Schneider, U. (1988). Concrete at high temperatures—a general review. *Fire Safety Journal*, 13, 55–68.
- Seleem, H. E. D. H., Rashad, A. M., & Elsokary, T. (2011). Effect of elevated temperature on physico-mechanical properties of blended cement concrete. *Construction and Building Materials*, 25, 1009–1017.
- Tai, Y.-S., Pan, H.-H., & Kung, Y.-N. (2011). Mechanical properties of steel fiber reinforced reactive powder concrete following exposure to high temperature reaching 800 °C. *Nuclear Engineering and Design*, 241, 2416–2424.
- Tao, J., Liu, X., Yuan, Y., & Taerwe, L. (2013). Transient strain of self-compacting concrete loaded in compression heated to 700 °C. *Materials and Structures*, 46, 191–201.
- Terro, M. J. (1998). Numerical modeling of the behavior of concrete structures in fire. *ACI Structural Journal*, 95, 183–193.
- Thienel, K.-C., & Rostasy, F. (1996). Transient creep of concrete under biaxial stress and high temperature. *Cement and Concrete Research*, 26, 1409–1422.
- Torelli, G., Mandal, P., Gillie, M., & Tran, V.-X. (2016). Concrete strains under transient thermal conditions: A state-of-the-art review. *Engineering Structures*, 127, 172–188.
- Wu, B., Siu-Shu Lam, E., Liu, Q., Chung, Y.-M., & Ho, F.-Y. (2010). Creep behavior of high-strength concrete with polypropylene fibers at elevated temperatures. *ACI Materials Journal*, 107, 2.
- Xing, W.-L., Shi, X.-D., & Ni, J.-G. (2011). Short-term thermal creep model of concrete based on experiments. *Engineering Mechanics*, 4, 027.
- Yu, K.-Q., Yu, J.-T., Dai, J.-G., Lu, Z.-D., & Shah, S. P. (2018). Development of ultra-high performance engineered cementitious composites using polyethylene (PE) fibers. *Construction and Building Materials*, 158, 217–227.
- Zheng, W., Li, H., & Wang, Y. (2012). Compressive behaviour of hybrid fiber-reinforced reactive powder concrete after high temperature. *Materials and Design*, 41, 403–409.
- Zheng, W., Luo, B., & Wang, Y. (2013). Compressive and tensile properties of reactive powder concrete with steel fibres at elevated temperatures. *Construction and Building Materials*, 41, 844–851.
- Zheng, W., Luo, B., & Wang, Y. (2014). Microstructure and mechanical properties of RPC containing PP fibres at elevated temperatures. *Magazine of Concrete Research*, 66, 397–408.
- Zheng, W., Luo, B., & Wang, Y. (2015). Stress-strain relationship of steel-fibre reinforced reactive powder concrete at elevated temperatures. *Materials and Structures*, 48, 2299–2314.

Publisher's Note

Springer Nature remains neutral with regard to jurisdictional claims in published maps and institutional affiliations.

Submit your manuscript to a SpringerOpen[®] journal and benefit from:

- Convenient online submission
- Rigorous peer review
- Open access: articles freely available online
- High visibility within the field
- Retaining the copyright to your article

Submit your next manuscript at ► [springeropen.com](https://www.springeropen.com)